Stable circular orbits in caged black hole spacetimes

Takahisa Igata[1,*] and Shinya Tomizawa[2,†]
[1]KEK Theory Center, Institute of Particle and Nuclear Studies, High Energy Accelerator Research Organization, Tsukuba 305-0801, Japan
[2]Mathematical Physics Laboratory, Toyota Technological Institute, Nagoya 468-8511, Japan

(Received 3 February 2021; accepted 8 March 2021; published 9 April 2021)

We consider the motion of massive and massless particles in a five-dimensional spacetime with a compactified extra-dimensional space where a black hole is localized, i.e., a caged black hole spacetime. We show the existence of circular orbits and reveal their sequences and stability. In the asymptotic region, stable circular orbits always exist, which implies that four-dimensional gravity is more dominant because of the small extra-dimensional space. In the vicinity of a black hole, they do not exist because the effect of compactification is no longer effective. We also clarify the dependence of the sequences of circular orbits on the size of the extra-dimensional space by determining the appearance of the innermost stable circular orbit and the last circular orbit (i.e., the unstable photon circular orbit).

DOI: 10.1103/PhysRevD.103.084011

I. INTRODUCTION

We naively perceive our world as a $(3+1)$-dimensional spacetime. However, in the context of unified theories, a higher-dimensional model of the Universe that adds an extra-dimensional space to the four-dimensional (4D) spacetime has been studied for a long time [1,2]. In this research background, higher-dimensional black holes have been actively studied as a field to find the various properties of higher-dimensional spacetime and gravity [3]. In understanding the nature of higher-dimensional black hole spacetimes, it is essential to consider test particle dynamics and compare it to that in 4D. As a first step, many studies were carried out on the motion of particles in an asymptotically flat higher-dimensional black hole spacetime with a single spherical horizon [4,5]. They revealed one of the most distinctive differences from 4D due to the dimensional dependence of gravity, the absence of the stable circular orbit [6–9].[1] As a result, the features of 4D gravity are gradually highlighted. Furthermore, since the uniqueness theorem does not hold for higher-dimensional black holes as in 4D [11,12], and they can have a nonspherical horizon (e.g., ring and lens spaces [13–15]), various particle dynamics depending on the horizon topology can also occur in higher dimensions. Indeed, stable circular/bound orbits appear in the five-dimensional (5D) black ring spacetime [16–21]. It was recently shown that stable circular/bound orbits also exist in the 5D supersymmetric black lens spacetimes [22,23].

The next step is to consider black hole spacetimes that model how we cannot observe an extra-dimensional space. One of the possible mechanisms to explain such inability is the compactification of the extra-dimensional space. Black hole spacetimes that incorporate this mechanism are called Kaluza-Klein black holes, and many solutions of this class have been found in the higher-dimensional Einstein gravity so far (see, e.g., Ref. [24] and references, therein). Focusing on 5D Kaluza-Klein black holes, we can classify them into two major classes. One is the class in which the horizon is spread out over the whole extra-dimensional space. The other is the class in which the horizon is localized in a certain portion of the extra-dimensional space, the so-called caged Kaluza-Klein black holes [25–28]. How the existence of a compact extra dimension has nontrivial effects on particle dynamics is an important and nontrivial question. Particle dynamics in the former class have been well studied [29–33] because of its relatively higher symmetry. On the other hand, particle dynamics in the latter class have not been well investigated because of its relatively lower symmetry.

However, it was recently shown that stable circular orbits exist by the many-body effect of black holes if the separation between the horizons is large enough in a 5D multiblack hole spacetime [34]. Since a caged black hole can be identified with an infinite number of black holes localized in a one-dimensional direction, such many-body effects can be expected to be inherited to particle dynamics in the caged black hole spacetime. The purpose of this paper is to reveal the effects of an extra dimension through

*igata@post.kek.jp
†tomizawa@toyota-ti.ac.jp

[1]Note that stable stationary/bound orbits can exist in the ultraspinning regime of the Myers-Perry black holes in more than six dimensions [10].

the dynamics of particles moving in the caged black hole backgrounds [25]. In the region sufficiently far from the black hole, the particle dynamics are like 4D, while in the near horizon, the effect that a black hole is localized in a compactified dimension appears more effectively.

This paper is organized as follows. In Sec. II, we introduce a 5D caged black hole spacetime and formulate conditions for stable/unstable circular orbits in the spacetime. In Sec. III, we clarify the dependence of sequences of circular orbits on the size of extra-dimensional space. Section IV is devoted to a summary and discussions. Throughout this paper, we use units in which $G = 1$ and $c = 1$, where G is the 5D Newton constant and c is the speed of light.

II. FORMULATION

We shortly review the caged black hole spacetime given in Ref. [25]. We begin by considering the metric and gauge field in the 5D Majumdar-Papapetrou geometry,

$$g_{\mu\nu}\mathrm{d}x^\mu \mathrm{d}x^\nu = -U^{-2}(\boldsymbol{x})\mathrm{d}t^2 + U(\boldsymbol{x})\mathrm{d}\boldsymbol{x}\cdot\mathrm{d}\boldsymbol{x}, \tag{1}$$

$$A_\mu \mathrm{d}x^\mu = -\frac{\sqrt{3}}{2}U^{-1}(\boldsymbol{x})\mathrm{d}t, \tag{2}$$

where t is the global Killing time, and $\boldsymbol{x}$ denotes spatial coordinates, and $\mathrm{d}\boldsymbol{x}\cdot\mathrm{d}\boldsymbol{x}$ is the metric in the 4D Euclidean space $\mathbb{E}^4$. For these ansatz, the only nontrivial components in the field equations are the (t,t) component of the Einstein equation and the t component of the Maxwell equation,[2] both of which are equivalent to the Laplace equation in $\mathbb{E}^4$,

$$\Delta_{\mathbb{E}^4} U = 0. \tag{4}$$

Let us introduce the coordinates $\boldsymbol{x} = (\rho, \theta, \phi, w)$ in which the Euclidean metric takes the form

$$\mathrm{d}\boldsymbol{x}\cdot\mathrm{d}\boldsymbol{x} = \mathrm{d}\rho^2 + \rho^2(\mathrm{d}\theta^2 + \sin^2\theta \mathrm{d}\phi^2) + \mathrm{d}w^2. \tag{5}$$

Consider a solution U of Eq. (4) for an infinite number of point sources of mass scale μ on the w-axis with equal spacing $a = 2\pi\ell$,

$$U = 1 + \sum_{n=-\infty}^{\infty} \frac{\mu}{\rho^2 + (w+na)^2} \tag{6}$$

$$= 1 + \frac{\pi\mu}{a\rho}\frac{\sinh(\pi\rho/a)\cosh(\pi\rho/a)}{\sin^2(\pi w/a) + \sinh^2(\pi\rho/a)} \tag{7}$$

$$= 1 + \frac{\mu}{2\ell\rho}\frac{\sin h(\rho/\ell)}{\cosh(\rho/\ell) - \cos(w/\ell)}, \tag{8}$$

where the dimension of μ is length squared even in ordinary units. This function has reflection symmetry under $w \to -w$. Furthermore, U is periodic in w with period a, and therefore, we may periodically identify the spacetime in the w direction. As a result, we have a spacetime where a single black hole with S^3 horizon topology is localized in a compactified extra dimension, which is referred to as the caged black hole spacetime. Thus, the parameter ℓ corresponds to the radius of the S^1-compactified extra-dimensional space. We only focus on the range $-\pi\ell < w \le \pi\ell$ in what follows.

We check the structure of the gravitational field of the caged black hole spacetime at several scales through the asymptotic shape of U. It is useful to gain an intuition for the dynamics of particles. In the region where $\rho, w \ll a$, the function U is expanded as

$$U = 1 + \frac{\mu}{r^2} + \frac{\pi^2}{3}\frac{\mu}{a^2} + O(\rho^2/a^2, w^2/a^2), \tag{9}$$

where $r^2 = \rho^2 + w^2$. The second term corresponds to the monopole term appearing in the case of 5D asymptotically flat black holes. The third term is contributions to the potential in the short-range from all the other image sources.[3] Therefore, we can expect that the particle dynamics in this region is the same as that in a 5D asymptotically flat black hole spacetime.

In the region where $\rho \gg a$, the function U is expanded as

$$U = 1 + \frac{\mu}{2\ell\rho} + \frac{\mu}{\ell\rho}e^{-\rho/\ell}\cos(w/\ell) + \cdots. \tag{11}$$

Note that the third and subsequent terms are exponentially suppressed, and thus, the metric reduces to a black string (ring). The power of ρ in the second term implies that test particles in the asymptotic region feel gravitational force as in 4D asymptotically flat black hole spacetimes.

We consider the dynamics of a freely falling particle with unit/zero mass in the caged black hole spacetime. Let p_μ be the canonical momenta conjugate with coordinate variables

[2]The field equations are derived from the 5D Einstein-Maxwell theory,

$$S = \int \mathrm{d}^5x\sqrt{-g}(R - F_{\mu\nu}F^{\mu\nu}), \tag{3}$$

where R is the Ricci tensor and $F_{\mu\nu}$ is the field strength of the gauge field.

[3]

$$\sum_{n=1}^{\infty}\frac{1}{n^2} = \frac{\pi^2}{6}. \tag{10}$$

of a particle. The Hamiltonian of affinely parametrized geodesics is given by

$$H = \frac{1}{2} g^{\mu\nu} p_\mu p_\nu = -\frac{U^2}{2} E^2 + \frac{1}{2U}\left(p_w^2 + p_\rho^2 + \frac{L^2}{\rho^2}\right), \quad (12)$$

where $E = -p_t$ is constant particle energy, and

$$L^2 = p_\theta^2 + \frac{p_\phi^2}{\sin^2\theta} \quad (13)$$

is a constant associated with the S^2 rotational symmetry. From the on-shell condition, $g^{\mu\nu} p_\mu p_\nu = -\kappa$, where κ is particle mass squared, we obtain the constraint equation

$$U^{-1}(\dot{\rho}^2 + \dot{w}^2) + V = E^2, \quad (14)$$

$$V(\rho, w; L^2) = \frac{L^2}{\rho^2 U^3} + \frac{\kappa}{U^2}, \quad (15)$$

where the dots denote the derivatives with respect to an affine parameter. We call V the effective potential of the two-dimensional (2D) dynamics in the (ρ, w) plane.

We focus on stationary orbits of particles with $\kappa = 1$, in which ρ and w remain constant. Note that all of the stationary orbits are circular because of the S^2 rotational symmetry. The conditions of the stationary orbits for V and $V_i = \partial_i V$ $(i = w, \rho)$ are written as

$$V_w = -\frac{2U_w}{U^3}\left(1 + \frac{3}{2}\frac{L^2}{\rho^2 U}\right) = 0, \quad (16)$$

$$V_\rho = -\frac{2L^2}{\rho^3 U^3} - \frac{2U_\rho}{U^3}\left(1 + \frac{3}{2}\frac{L^2}{\rho^2 U}\right) = 0, \quad (17)$$

$$V = E^2, \quad (18)$$

where the explicit forms of $U_i = \partial_i U$ $(i = w, \rho)$ are given by

$$U_w = -\frac{\mu}{2\ell^2\rho}\frac{\sin(w/\ell)\sinh(\rho/\ell)}{[\cos(w/\ell) - \cosh(\rho/\ell)]^2}, \quad (19)$$

$$U_\rho = \frac{\mu}{2\ell^2\rho^2}\frac{\rho[1 - \cos(w/\ell)\cosh(\rho/\ell)] + \ell\sinh(\rho/\ell)[\cos(w/\ell) - \cosh(\rho/\ell)]}{[\cos(w/\ell) - \cosh(\rho/\ell)]^2}. \quad (20)$$

The condition (16) leads to $U_w = 0$, i.e.,

$$w = 0, \ \ \pi\ell. \quad (21)$$

These correspond to the fixed points of the reflection symmetry of U. Furthermore, solving the conditions (17) and (18) for L^2 and E^2, we obtain

$$L^2 = L_0^2(\rho, w) \coloneqq -\frac{2\rho^3 U U_\rho}{f}, \quad (22)$$

$$E^2 = E_0^2(\rho, w) \coloneqq V(\rho, w; L_0^2) = \frac{2U + \rho U_\rho}{f U^2}, \quad (23)$$

where

$$f(\rho, w) = 2U + 3\rho U_\rho. \quad (24)$$

These must be non-negative to find circular orbits on $w = 0$ or $\pi\ell$. Therefore, we can represent the sequence of circular orbits on the (ρ, w) plane as

$$\gamma_0 = \{(\rho, w) | (w = 0 \quad \text{or} \quad w = \pi\ell), L_0^2 \geq 0\}, \quad (25)$$

where we have used the fact that $L^2 \geq 0$ always means $E^2 > 0$ because of Eqs. (14) and (15). The explicit forms of L_0^2 and E_0^2 on γ_0 are given by

$$L_0^2(\rho, \Theta(\sigma)\pi\ell) = \frac{\mu\rho}{\ell}\frac{[-\sigma\rho + \ell\sinh(\rho/\ell)][2\ell\rho + \mu(\tanh[\rho/(2\ell)])^\sigma]}{4\ell^2\rho\cosh(\rho/\ell) - \mu\ell\sinh(\rho/\ell) + \sigma(3\mu + 4\ell^2)\rho}, \quad (26)$$

$$E_0^2(\rho, \Theta(\sigma)\pi\ell) = \frac{4\ell^2\rho^2(\mu[\sigma\rho + \ell\sinh(\rho/\ell)] + 4\ell^2\rho[\sigma + \cosh(\rho/\ell)])}{[2\ell\rho + \mu(\tanh[\rho/(2\ell)])^\sigma]^2[4\ell^2\rho\cosh(\rho/\ell) - \mu\ell\sinh(\rho/\ell) + \sigma(3\mu + 4\ell^2)\rho]}, \quad (27)$$

respectively, where $\sigma = \pm 1$, and $\Theta(\sigma)$ denotes the Heaviside step function, and we have used

$$f(\rho, \Theta(\sigma)\pi\ell) = 2 - \frac{\mu}{4\ell^2\rho}\frac{-3\sigma\rho + \ell\sinh(\rho/\ell)}{\Theta(\sigma)\cosh^2[\rho/(2\ell)] + \Theta(-\sigma)\sinh^2[\rho/(2\ell)]}. \quad (28)$$

The sign of $f(\rho,\Theta(\sigma)\pi\ell)$ determines the signs of $L_0^2(\rho,\Theta(\sigma)\pi\ell)$ and $E_0^2(\rho,\Theta(\sigma)\pi\ell)$. They diverge at $f(\rho,\Theta(\sigma)\pi\ell)=0$.

We further classify γ_0 by imposing stability conditions for circular orbits. Let (V_{ij}) be the Hessian matrix of V on the 2D flat space with $\delta_{ij}dx^i dx^j = d\rho^2 + dw^2$, where $V_{ij} = \partial_j\partial_i V$ $(i,j=\rho,w)$. Let h and k be the determinant and the trace of (V_{ij}) on $\mathbb{E}^2$, i.e., $h(\rho,w;L^2)=\det(V_{ij})$ and $k(\rho,w;L^2)=\mathrm{tr}(V_{ij})$, respectively. Since we analyze the particle dynamics on a 2D reduced space, of which metric is $\tilde{\gamma}_{ij}=\Omega^2\delta_{ij}=U^{-1}\delta_{ij}$ [see Eq. (14)], then the stability of circular orbits should be determined on the basis of the Hessian matrix $(\tilde{V}_{ij})=(\tilde{\nabla}_j\tilde{\nabla}_i V)$ in the 2D conformally flat space, where $\tilde{\nabla}_i$ is the covariant derivative associated with $\tilde{\gamma}_{ij}$. Focus on the relation between $\tilde{V}_{ij}$ and V_{ij},

$$\tilde{V}_{ij} = V_{ij} - \Omega^{-1}(2V_{(i}\Omega_{j)} - \delta_{ij}\delta^{kl}V_k\Omega_l), \tag{29}$$

where $\Omega_i=\partial_i\Omega$. Note that $\tilde{V}_{ij}=V_{ij}$ on γ_0 because $V_i=0$ there. Furthermore, on γ_0, the trace and determinant of $(\tilde{V}_{ij})$ coincide with Uk and U^2h, respectively. Therefore, we can use k and h to determine the signs of the trace and determinant of $(\tilde{V}_{ij})$, respectively. In terms of them, we define the region D such that

$$D=\{(\rho,w)|h_0>0,k_0>0,L_0^2>0\}, \tag{30}$$

where h_0 and k_0 are defined as

$$h_0(\rho,w) \coloneqq h(\rho,w;L_0^2)|_{U_w=0} = \frac{-16\rho U^2U_{w\rho}^2 + 8U_{ww}[6\rho UU_\rho^2 + 3\rho^2U_\rho^3 + 2U^2(3U_\rho+\rho U_{\rho\rho})]}{\rho U^6 f^2}, \tag{31}$$

$$k_0(\rho,w) \coloneqq k(\rho,w;L_0^2)|_{U_w=0} = -\frac{2}{\rho U^4}\frac{6\rho UU_\rho^2 + 3\rho^2U_\rho^3 + 2U^2(3U_\rho+\rho U_{\rho\rho}+\rho U_{ww})}{f}. \tag{32}$$

The restriction that $U_w=0$ means that the terms proportional to U_w have been removed. As a result, the part of γ_0 overlapped by D is the sequence of stable circular orbits, and its boundaries correspond to the marginally stable circular orbits. On the other hand, the part of γ_0 without overlap with D is the sequence of unstable circular orbits.

III. CIRCULAR ORBITS IN THE CAGED BLACK HOLE SPACETIMES

We consider circular orbits in the 5D caged black hole spacetimes by using the quantities introduced in the previous section. First, we illustrate typical sequences of circular orbits by comparing the size of the extra dimension a and the mass parameter μ. We use units in which $\mu=1$ in what follows. Figure 1(a) shows the case $a=5$, typical sequences of circular orbits for $a\gg 1$. The black solid lines are γ_0, and the blue shaded region is D. The part of γ_0 overlapped by D appears on $w=0$, a sequence of stable circular orbits, which extends from the innermost stable circular orbit (ISCO) $\rho=\rho_{\mathrm{I}}$ (indicated by a red dot) to infinity. The energy and squared angular momentum, E_0 and L_0^2, decrease monotonically with ρ (i.e., $dE_0(\rho,0)/d\rho\geq 0$ and $dL_0^2(\rho,0)/d\rho\geq 0$) in the

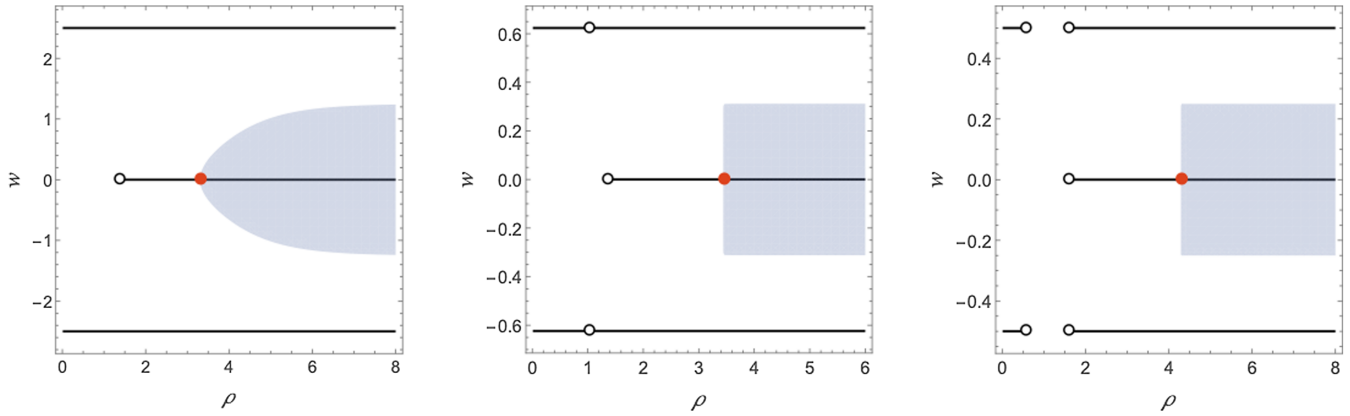

(a) $a=5$ (b) $a=a_1=1.2470\ldots$ (c) $a=1$

FIG. 1. Sequences of stable/unstable circular orbits for several sizes of the extra dimension. We use units in which $\mu=1$. Black solid lines show γ_0, sequences of circular orbits, and blue shaded regions show D, inside which circular orbits are stable. Red dots denote the ISCOs, and white circles denote UPCOs.

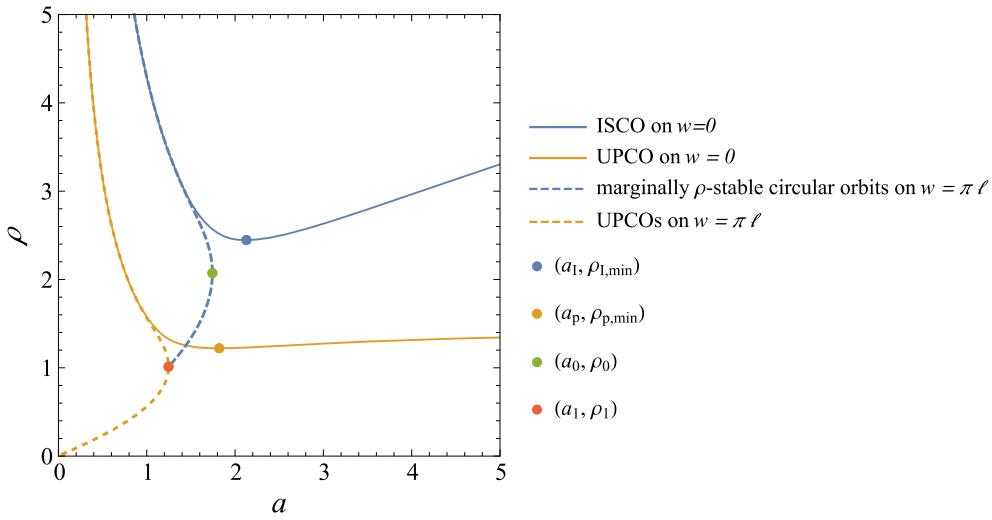

FIG. 2. Dependence of the radii of the ISCO, UPCOs, and marginally ρ-stable circular orbits on the size of the extra dimension, a. We use units in which $\mu = 1$. Blue solid curve denotes the radius of the ISCO on $w = 0$. Blue dashed curve denotes a pair of radii of marginally ρ-stable circular orbits on $w = \pi\ell$. Orange solid and dashed curves show the radii of UPCOs on $w = 0$ and $w = \pi\ell$, respectively.

range $\rho_{\rm I} \le \rho < \infty$. Each of them takes a local minimum value at the ISCO, where $h_0(\rho_{\rm I}, 0) = 0$ also holds. On the other hand, a sequence of unstable circular orbits appears on the segment of γ_0 between the ISCO and the last circular orbit $\rho = \rho_{\rm p}$ (denoted by a white circle). In this range, the energy and squared angular momentum satisfy $\mathrm{d}E_0(\rho, 0)/\mathrm{d}\rho < 0$ and $\mathrm{d}L_0^2(\rho, 0)/\mathrm{d}\rho < 0$, respectively, and diverge in the limit to the white circle. The last circular orbit on $w = 0$ is justified as an unstable photon circular orbit (UPCO)[4] because the ratio L_0/E_0 is still finite even in the limit. We also find a sequence of unstable circular orbits on $w = \pi\ell$. Next, let us see the case where a takes a smaller value. Figure 1(b) shows the case $a = a_1$, where E_0 and L_0^2 on $w = \pi\ell$ diverge at a radius $\rho = \rho_1$ (white circle), where

$$a_1 = 1.2470\ldots, \tag{33}$$

$$\rho_1 = 1.0129\ldots. \tag{34}$$

It corresponds to a UPCO on $w = \pi\ell$. Figure 1(c) shows the case $a = 1$, typical sequences of circular orbits for $a \lesssim 1$. Even in the range, we can see a sequence of stable circular orbits between infinity and the ISCO on $w = 0$ and can also see a sequence of unstable circular orbits between the ISCO and the last circular orbit (i.e., the UPCO). The difference appears in sequences on $w = \pi\ell$, which separate into two pieces. Each end point of the sequences corresponds to a UPCO.

[4]The conventional term "photon" is used to describe the unstable circular orbit of a massless particle.

Figure 2 shows the dependence of some characteristic orbital radii on a. The blue solid curve shows the ISCO radius $\rho = \rho_{\rm I}$ as a function of a, which is determined by $h_0(\rho_{\rm I}, 0) = 0$. For $a > a_{\rm I}$, the radius $\rho_{\rm I}$ monotonically decreases as a decreases, whereas for $a < a_{\rm I}$, it monotonically increases as a decreases, where

$$a_{\rm I} = 2.1286\ldots. \tag{35}$$

Hence, at $a = a_{\rm I}$, the ISCO radius takes the minimum value (see the blue dot)

$$\rho_{\rm I,min} = 2.4465\ldots. \tag{36}$$

The orange solid curve shows the last circular orbit radius $\rho = \rho_{\rm p}$ (or equivalently, the UPCO radius) as a function of a, which is determined by $f(\rho_{\rm p}, 0) = 0$. For $a > a_{\rm p}$, the radius $\rho_{\rm p}$ monotonically decreases as a decreases, whereas for $a < a_{\rm p}$, it monotonically increases as a decreases, where

$$a_{\rm p} = 1.8206\ldots. \tag{37}$$

At $a = a_{\rm p}$, the radius of the UPCO on $w = 0$ takes the minimum value (see the orange dot)

$$\rho_{\rm p,min} = 1.2210\ldots. \tag{38}$$

The blue dashed curve shows a pair of circular orbit radii on $w = \pi\ell$ that are marginally stable against small perturbations only in the ρ direction, which are determined by $V_{\rho\rho}(\rho, \pi\ell; L_0^2(\rho, \pi\ell)) = 0$. We call them marginally ρ-stable circular orbits. The outer radius $\rho \ge \rho_0$ appears only in the range $0 < a \le a_0$, where

$$a_0 = 1.7430\ldots, \tag{39}$$

$$\rho_0 = 2.0717\ldots, \tag{40}$$

and increases as a decreases. The inner radius $\rho \le \rho_0$ appears only in the range $a_1 < a < a_0$ and decreases with a and disappears at $a = a_1$. The orange dashed curve shows a pair of the radii of UPCOs on $w = \pi\ell$. The inner radius decreases with a and finally goes to zero in the limit $a \to 0$. The outer radius increases as a decreases. There are no circular orbits between these radii. In the enclosed region by the blue and orange dashed curves, the circular orbits that are unstable in all directions appear on $w = \pi\ell$, and the energy and squared angular momentum satisfy $\mathrm{d}E_0(\rho, \pi\ell)/\mathrm{d}\rho < 0$ and $\mathrm{d}L_0^2(\rho, \pi\ell)/\mathrm{d}\rho < 0$, respectively. In the region to the right of all the dashed curves, ρ-stable circular orbits appear on $w = \pi\ell$, and the energy and squared angular momentum satisfy $\mathrm{d}E_0(\rho, \pi\ell)/\mathrm{d}\rho > 0$ and $\mathrm{d}L_0^2(\rho, \pi\ell)/\mathrm{d}\rho > 0$, respectively.

Consider the qualitative behaviors of particle dynamics in the asymptotic analysis of V. We restore μ in the following discussions. We can see that V in the asymptotic region $\rho \gg a$ behaves like the effective potential of a 4D asymptotically flat black hole spacetime, as is expected from Eq. (11), as

$$V = 1 - \frac{\mu}{\ell\rho} + \frac{L^2}{\rho^2} - \frac{3\mu L^2}{2\ell\rho^3} + O(\ell e^{-\rho/\ell}/\rho). \tag{41}$$

The second term implies that the gravitational mass of the black hole, as perceived by the particle, is proportional to $M_{\mathrm{grav}} = \mu c^2/(2\ell G_4)$, where we have restored the speed of light c and the 4D Newton constant $G_4 = G/a$. Hence, the mass increases as ℓ decreases. Evaluating the ISCO radius up to this order, we find $\rho_{\mathrm{I}} = (9/2)(\mu/\ell) = (9/2)r_{\mathrm{g}}$, where $r_{\mathrm{g}} = 2G_4 M_{\mathrm{grav}}/c^2$ is the Schwarzschild radius. Furthermore, as can be seen from the fact that the leading terms in Eq. (41) are independent of w, gravitational force in the ρ direction is dominant in the asymptotic region. As a result, the ISCO and the marginally ρ-stable circular orbit radii there increase as a decreases, and they must have the same value regardless of w, i.e., in this region, the solid and dashed blue curves in Fig. 2 coincide with each other. The same behavior can be seen for UPCOs, i.e., the solid and dashed orange curves coincide with each other in this region.

We find from Eq. (9) that V in the range $\rho, w \ll a$ behaves like the effective potential of a 5D asymptotically flat black hole spacetime as

$$V = 1 - \frac{2\pi^2}{3}\frac{\mu}{a^2} - \frac{2\mu}{\rho^2 + w^2} + \left(1 - \frac{\pi^2\mu}{a^2}\right)\frac{L^2}{\rho^2} - \frac{3\mu L^2}{\rho^2(\rho^2 + w^2)} + O(\rho^2/a^2, w^2/a^2). \tag{42}$$

The third term corresponds to a 5D gravitational potential. In particular, on $w = 0$, the potential V of Eq. (42) reduces to

$$V(\rho, 0) = 1 - \frac{2\pi^2}{3}\frac{\mu}{a^2} + \frac{(1 - \pi^2\mu/a^2)L^2 - 2\mu}{\rho^2} - \frac{3\mu L^2}{\rho^4} + O(\rho^2/a^2). \tag{43}$$

Thus, we find that there are no circular orbits in this range because the third and fourth terms cannot make a potential well.

IV. SUMMARY AND DISCUSSIONS

We have considered sequences of circular orbits for massive and massless particles in the 5D caged black hole spacetime, in which a black hole is localized in the extra-dimensional space. We have given a systematic way to find stationary orbits (i.e., circular orbits) and a prescription to determine whether they are stable or unstable. Using these, we have identified a typical sequence of circular orbits for each size of extra-dimensional space and have specified the part where it shows stable behavior.

We have found that stable circular orbits exist in the asymptotic region regardless of the scales of the extra dimension and the black hole mass. It implies that the localization effect of the black hole in the extra-dimensional space does not appear in the region far from the black hole. The existence of stable circular orbits in such an asymptotic region is analogous to the case of a 4D asymptotically flat black hole spacetime, rather than a 5D asymptotically flat black hole spacetime with a spherical horizon. In other words, we can interpret the effect of the compactification of the extra-dimensional space in the asymptotic region as reproducing effective 4D gravity. As mentioned in the Introduction, we can also interpret this phenomenon as a consequence of the many-body effect due to the infinite images of a black hole [34]. On the other hand, in the region closer to the black hole than the size of the extra dimension, stable circular orbits do not appear because 5D gravity of the asymptotically flat black hole spacetime dominates due to the suppression of the compactification effect. In the intermediate region between these two, the sequence of stable circular orbits reaches the ISCO and switches to the unstable circular orbits, and finally, it terminates in the last circular orbit (i.e., the UPCO). This behavior does not qualitatively depend on the extra-dimensional size, but the ISCO and UPCO take various radii according to the sizes of mass and compactification.

It is inadvisable to apply this model to the Universe because the caged black hole has an electric charge and is

justified only at $a/\sqrt{\mu} \gg 1$[5] (see, e.g., Ref. [35]). Even if we applied it, we would find that the behavior at infinity is the same as in 4D, but for example, the ISCO radius takes a larger value $4.5r_g$ than the value $3r_g$ we expect, where r_g is the Schwarzschild radius. Such behavior does not adequately represent the actual astrophysical situation. If we consider the higher-dimensional Universe scenario in an astrophysical situation, then we may give a more realistic model by a squashed Kaluza-Klein black hole with a horizon expanding to the whole extra dimension, rather than a caged black hole. The interpretation of stable circular orbits proposed recently in the context of the AdS/CFT correspondence would also be interesting [36,37]. These issues deserve further study.

[5]

$$\frac{a}{\sqrt{\mu}} \sim 10^{-4}\left(\frac{M_\odot}{M_{\rm grav}}\right)^{1/2}\left(\frac{a}{0.1\ {\rm mm}}\right)^{1/2} \sim 10^{23}\left(\frac{{\rm TeV}/c^2}{M_{\rm grav}}\right)^{1/2}\left(\frac{a}{0.1\ {\rm mm}}\right)^{1/2}. \quad (44)$$

ACKNOWLEDGMENTS

This work was supported by the Grant-in-Aid for Early-Career Scientists [JSPS KAKENHI Grant No. JP19K14715 (T. I.)] and Grant-in-Aid for Scientific Research (C) [JSPS KAKENHI Grant No. JP17K05452 (S. T.)] from the Japan Society for the Promotion of Science. S. T. is also supported from Toyota Technological Institute Fund for Research Promotion A.

[1] T. Kaluza, On the problem of unity in physics, Sitzungsber. Preuss. Akad. Wiss. Berlin (Math. Phys.) **1921**, 966 (1921); Int. J. Mod. Phys. D **27**, 1870001 (2018).
[2] O. Klein, Quantum theory and five-dimensional theory of relativity, Z. Phys. **37**, 895 (1926).
[3] R. Emparan and H. S. Reall, Black holes in higher dimensions, Living Rev. Relativity **11**, 6 (2008).
[4] F. R. Tangherlini, Schwarzschild field in n dimensions and the dimensionality of space problem, Nuovo Cimento **27**, 636 (1963).
[5] R. C. Myers and M. J. Perry, Black holes in higher dimensional space-times, Ann. Phys. (N.Y.) **172**, 304 (1986).
[6] E. Hackmann, V. Kagramanova, J. Kunz, and C. Lammerzahl, Analytic solutions of the geodesic equation in higher dimensional static spherically symmetric space-times, Phys. Rev. D **78**, 124018 (2008).
[7] V. P. Frolov and D. Stojkovic, Particle and light motion in a space-time of a five-dimensional rotating black hole, Phys. Rev. D **68**, 064011 (2003).
[8] V. Diemer, J. Kunz, C. Lämmerzahl, and S. Reimers, Dynamics of test particles in the general five-dimensional Myers-Perry spacetime, Phys. Rev. D **89**, 124026 (2014).
[9] V. Cardoso, A. S. Miranda, E. Berti, H. Witek, and V. T. Zanchin, Geodesic stability, Lyapunov exponents and quasinormal modes, Phys. Rev. D **79**, 064016 (2009).
[10] T. Igata, Stable bound orbits in six-dimensional Myers-Perry black holes, Phys. Rev. D **92**, 024002 (2015).
[11] S. Hollands and S. Yazadjiev, Uniqueness theorem for 5-dimensional black holes with two axial Killing fields, Commun. Math. Phys. **283**, 749 (2008).
[12] S. Hollands and A. Ishibashi, Black hole uniqueness theorems in higher dimensional spacetimes, Classical Quantum Gravity **29**, 163001 (2012).
[13] R. Emparan and H. S. Reall, A Rotating Black Ring Solution in Five-dimensions, Phys. Rev. Lett. **88**, 101101 (2002).
[14] H. K. Kunduri and J. Lucietti, Supersymmetric Black Holes with Lens-Space Topology, Phys. Rev. Lett. **113**, 211101 (2014).
[15] S. Tomizawa and M. Nozawa, Supersymmetric black lenses in five dimensions, Phys. Rev. D **94**, 044037 (2016).
[16] J. Hoskisson, Particle motion in the rotating black ring metric, Phys. Rev. D **78**, 064039 (2008).
[17] T. Igata, H. Ishihara, and Y. Takamori, Stable bound orbits around black rings, Phys. Rev. D **82**, 101501 (2010).
[18] S. Grunau, V. Kagramanova, J. Kunz, and C. Lammerzahl, Geodesic motion in the singly spinning black ring space-time, Phys. Rev. D **86**, 104002 (2012).
[19] T. Igata, H. Ishihara, and Y. Takamori, Stable bound orbits of massless particles around a black ring, Phys. Rev. D **87**, 104005 (2013).
[20] T. Igata, Particle dynamics in the Newtonian potential sourced by a homogeneous circular ring, Phys. Rev. D **101**, 124064 (2020).
[21] T. Igata, Chaotic particle motion around a homogeneous circular ring, Phys. Rev. D **102**, 044019 (2020).
[22] S. Tomizawa and T. Igata, Stable bound orbits around a supersymmetric black lens, Phys. Rev. D **100**, 124031 (2019).
[23] S. Tomizawa and T. Igata, Stable bound orbits in black lens backgrounds, Phys. Rev. D **102**, 124079 (2020).
[24] S. Tomizawa and H. Ishihara, Exact solutions of higher dimensional black holes, Prog. Theor. Phys. Suppl. **189**, 7 (2011).
[25] R. C. Myers, Higher dimensional black holes in compactified space-times, Phys. Rev. D **35**, 455 (1987).
[26] B. Kol, E. Sorkin, and T. Piran, Caged black holes: Black holes in compactified space-times. 1. Theory, Phys. Rev. D **69**, 064031 (2004).
[27] T. Harmark, Small black holes on cylinders, Phys. Rev. D **69**, 104015 (2004).

[28] R. Suzuki, S. Kinoshita, and T. Shiromizu, Caged black hole with Maxwell charge, Phys. Rev. D **86**, 044018 (2012).
[29] P. H. Lim and P. S. Wesson, The perihelion problem in Kaluza-Klein gravity, Astrophys. J. **397**, L91 (1992).
[30] D. Kalligas, P. S. Wesson, and C. W. F. Everitt, The classical tests in Kaluza-Klein gravity, Astrophys. J. **439**, 548 (1995).
[31] H. Liu and J. M. Overduin, Solar system tests of higher dimensional gravity, Astrophys. J. **538**, 386 (2000).
[32] K. Matsuno and H. Ishihara, Geodetic precession in squashed Kaluza-Klein black hole spacetimes, Phys. Rev. D **80**, 104037 (2009).
[33] F. Long, J. Wang, S. Chen, and J. Jing, Shadow of a rotating squashed Kaluza-Klein black hole, J. High Energy Phys. 10 (2019) 269.
[34] T. Igata and S. Tomizawa, Stable circular orbits in higher-dimensional multi–black hole spacetimes, Phys. Rev. D **102**, 084003 (2020).
[35] T. Harmark and N. A. Obers, Black holes on cylinders, J. High Energy Phys. 05 (2002) 032.
[36] D. Berenstein, Z. Li, and J. Simón, ISCOs in AdS/CFT, Classical Quantum Gravity **38**, 045009 (2021).
[37] R. A. Konoplya and A. Zhidenko, Massive particles in the Einstein-Lovelock-anti-de Sitter black hole spacetime, Classical Quantum Gravity **38**, 045015 (2021).